ChemComm
Chemical Communications

Accepted Manuscript

This article can be cited before page numbers have been issued, to do this please use: P. Lama, A. Hazra and L. Barbour, *Chem. Commun.*, 2019, DOI: 10.1039/C9CC06634A.

ROYAL SOCIETY OF CHEMISTRY

rsc.li/chemcomm

Cite this: DOI: 10.1039/c0xx00000x

www.rsc.org/xxxxxx

ARTICLE TYPE

Accordion and layer-sliding motion to produce anomalous thermal expansion behaviour in 2D-coordination polymers

Prem Lama,*[a] Arpan Hazra[b] and Leonard J. Barbour*[b]

[a]School of Chemical Sciences, Goa University, Taleigao Plateau, Taleigao 403206, Goa, India.
[b]Department of Chemistry and Polymer Science, University of Stellenbosch, Matieland 7602, Stellenbosch, South Africa

Received (in XXX, XXX) Xth XXXXXXXXX 20XX, Accepted Xth XXXXXXXXX 20XX
DOI: 10.1039/b000000x

Solvent-free (1) and solvated (2) 2D-coordination polymers have been synthesised by varying the amount of solvent during crystallisation. 1 undergoes a unique accordion motion of 2D zig-zag interwoven layers whereas 2 experiences layer-sliding within 2D layers to produce anomalous thermal expansion behaviour.

Positive thermal expansion (PTE) is observed for most materials and is generally due to longitudinal vibrational motion, which leads to expansion (~20 MK^{-1}) along three orthogonal directions with increasing temperature.[1] However, there are reports of fascinating mechanical responses such as hinge-like[2] and stretching-tilting[3] motion of molecules, associated with particular arrangements in the solid state that can induce colossal PTE (> 100 MK^{-1}), negative thermal expansion (NTE)[4] or zero thermal expansion (ZTE)[5] (i.e., anomalous thermal behaviour). Commonly, anomalous behaviour in metal-organic materials occurs as a result of structural flexibility,[6] which could be due to the choice of metal ions, ligands or both. In recent years much attention has been devoted to fully understanding such thermoresponsive behaviour of materials. Indeed, a large number of interesting mechanisms have been reported for anomalous behaviour in metal oxides[7] and organic compounds.[8] However, similar reports for coordination polymers (CPs) are also increasing in number with ever growing interest in the properties of such materials.[9] This is particularly so because the topologies and properties of CPs can easily be tuned by varying the metal ions and the types of ligand that can facilitate more flexibility of the system.[10] In this regard, single crystal X-ray diffraction (SCXRD) at variable temperature provides direct insight towards understanding the structural dynamics and mechanisms involved.[3]

We have investigated two related 2D CPs with a view to understanding the anomalous nature of their thermal expansion behaviour. The CPs $[Zn(tp)(bpp)]_n$ (**1**, solvent free form) and $\{[Zn(tp)(bpp)_{0.5}]\cdot 0.5dmf\}_n$ (**2**, solvated form) (Scheme S1), (tp = terepthalate, bpp = 1,3-bis(4-pyridyl)propane and dmf = *N*,*N*'-dimethyl formamide) were synthesised using a modified literature procedure by varying the amount of solvent (Scheme S1, Table S1-S5).[11] SCXRD analysis at 100 K reveals that **1** crystallises in the centrosymmetric orthorhombic space group *Pbca*. The asymmetric unit consists of one Zn^{2+} ion, one tp ligand and one bpp ligand. The Zn^{2+} ion adopts a distorted tetrahedral coordination geometry, binding to two monodentate carboxylate oxygen atoms from two separate tp ligands, and to pyridyl units of two bpp ligands (Fig. S1). The tetrahedral Zn^{2+} centres are linked by the bpp and tp ligands along the crystallographic *a* and *c* axes, respectively, thus forming two-dimensional zig-zag layers (Fig. 1). Pairs of neighbouring layers interpenetrate to yield an interwoven twofold sheet with several C-H$\cdots\pi$ interactions between the two

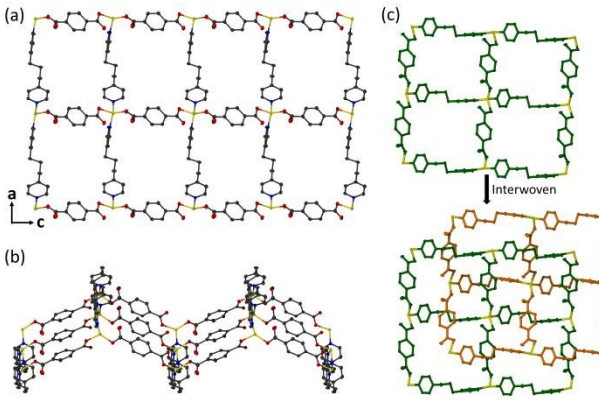

Fig. 1 Perspective views of **1**. (a) A single 2D layer parallel to (010). (b) Zig-zag layers formed by carboxylate and bpp ligands. (c) Each 2D layer is interwoven with another layer to form a twofold interwoven sheet. All hydrogen atoms have been omitted for clarity.

constituent layers (Fig. 1c, Figs. S2-S3, Table S6). There are also weak $\pi\cdots\pi$ interactions between the aromatic rings of the carboxylate and pyridyl units of neighbouring twofold-interwoven sheets (Fig. 2, Table S7), owing to which the interwoven sheets stack on one another to generate the overall 3D architecture (Figure S4).

View Article Online
DOI: 10.1039/C9CC06634A

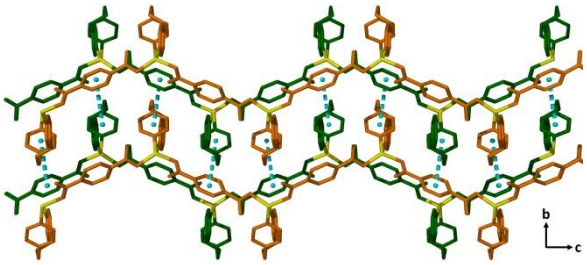

Fig. 2 Perspective view of **1** along [100] showing the $\pi\cdots\pi$ stacking between the two zig-zag interwoven layers. Hydrogen atoms have been omitted for clarity.

Variable-temperature single-crystal X-ray diffraction (VT-SCXRD) experiments were carried out with a view to understanding temperature-dependent structural changes of **1**. Starting at 260 K, the crystal was cooled to 100 K and intensity data were collected at 20 K intervals. Upon cooling, the crystallographic *b* axis contracts significantly, the *c* axis elongates slightly, and the *a* axis remains almost constant (Fig. 3). The linear thermal expansion coefficients along the three perpendicular crystallographic axes *a*, *b* and *c* are 0.1(2), 103.8(2) and −10.6(2) MK^{-1}, respectively. Thus **1** shows a rare combination of zero, positive and negative thermal expansion behaviour.[12,7b,9a] The overall volumetric thermal expansion coefficient is 93.1(3) MK^{-1} (Fig S5). The reversibility of the thermal expansion process was confirmed by first cooling the crystal from 260 to 100 K and then heating it again to 260 K (**1_260K-R** in ESI). The initial and final unit cell dimensions at 260 K agree within experimental error. Differential scanning calorimetry (DSC) shows no thermal event in the temperature range of 100 to 260 K, confirming that **1** does not undergo any phase change in this range (Fig. S6). Thermogravimetric analysis (TGA) shows that the compound **1** is thermally stable up to 350 °C, beyond which it starts to decompose (Fig. S7).

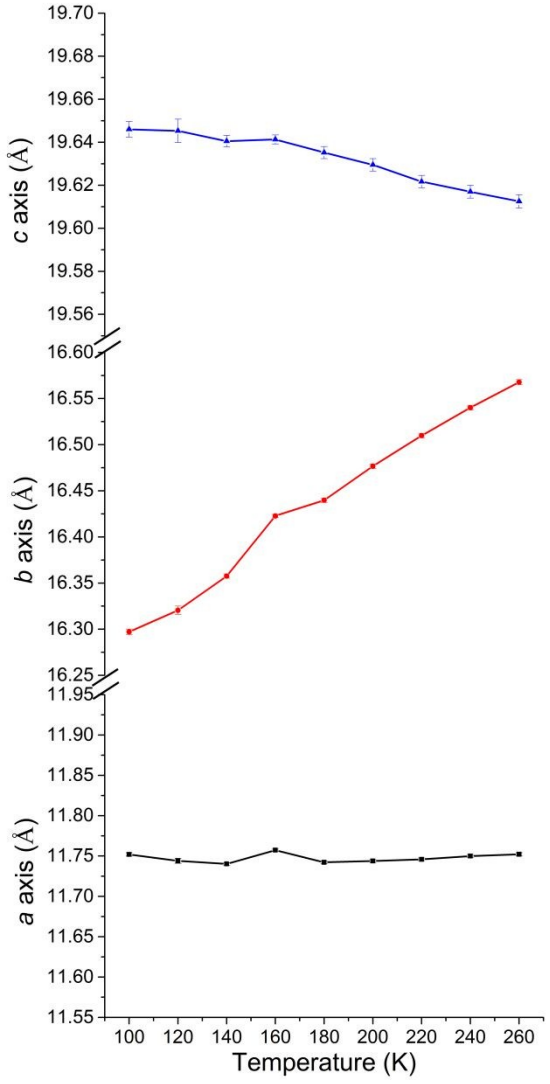

Fig. 3 Variation of unit cell dimensions of **1** (including error bars) with temperature.

In order to elucidate the mechanism responsible for the anomalous thermal expansion properties of **1**, we analysed the types of intermolecular interactions and temperature-dependent structural changes. Upon cooling, the intermolecular C-H$\cdots\pi$ interactions (Figs. S2-S3) within an interwoven sheet strengthen, as is evident from the decrease of the non-bonding distances C4$\cdots i3$ and C10$\cdots i1$ ($i1$ = centroid of C2-C7 and $i3$ = centroid of N2,C17-C21, Table S6). This effect enhances positive thermal expansion along the *b* axis. In addition, the $\pi\cdots\pi$ interaction distance $i1\cdots i3$ between neighbouring twofold-interwoven sheets also decreases on cooling (Table S7). Since these interactions are aligned almost parallel to the crystallographic *b* axis (Fig. 2), they also contribute to the overall colossal positive thermal expansion along [010]. Close examination of the corrugated 2D layers parallel to (010) shows that the distance between the Zn^{2+} ions connected by bpp ligands along the crystallographic *a* axis remains practically constant, thus resulting in zero thermal expansion along [100]. This occurs despite gradual twisting of the flexible alkyl chain of the bpp unit with temperature (Fig. S8, Table S8). The C-H$\cdots\pi$ interaction C21$\cdots i2$ ($i2$ = centroid of N1,C9-C13) aligns almost parallel to the *c* axis, which shows slight expansion on cooling (Fig S2, Table S6). At the same time, the non-bonding metal-metal distance (d2) across the tp linkage (i.e. along *c*) undergoes slight expansion with decreasing temperature (Fig. 4, Table S9). Since d1 remains almost constant, elongation of d2 is due to the slight overall increase in the angle θ_1 with cooling, and hence negative thermal expansion is observed along the crystallographic *c* axis. In general, within the 2D zig-zag layer the structure remains largely unchanged along the *a* axis, whereas it undergoes slight contraction along *c* with increasing temperature. This kind of deformation of a 2D zig-zag layer is best described as accordion[13] motion (Video 1).

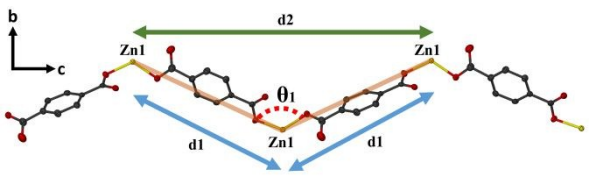

Fig. 4 Perspective view showing the non-bonding distance (d2) and angle (θ_1) that are affected by anomalous thermal expansion in **1**.

View Article Online
DOI: 10.1039/C9CC06634A

SCXRD analysis at 100 K reveals that **2** crystallises in the monoclinic space group $P2_1/m$. The asymmetric unit consists of one Zn^{2+} ion, one tp ligand, half a bpp ligand and a half-occupancy

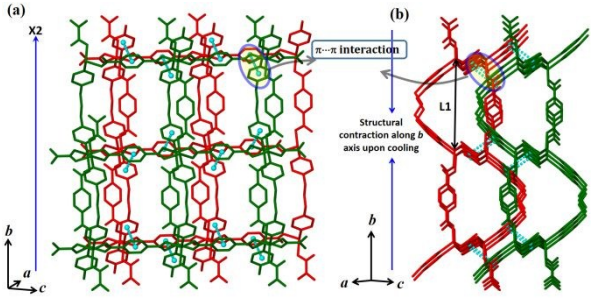

Fig 5: (a) Perspective views of the $\pi\cdots\pi$ interactions between aromatic groups of the carboxylate and pyridyl of two adjacent layers in **1**. (b) $\pi\cdots\pi$ interactions become stronger upon cooling and thus contraction along the *b* axis (also *X2*) results in positive thermal expansion. The distance between the Zn^{2+} atoms connected by the bpp ligand along the *b* axis (L1) decreases upon cooling.

dmf molecule. The Zn^{2+} ion in **2** adopts a distorted tetrahedral coordination geometry unlike that of **1**; it is coordinated to three carboxylate groups, each in monodentate mode, with the remaining position occupied by a pyridyl unit of bpp (Fig. S9a). Two such Zn^{2+} ions form a dimeric unit, within which they are connected by two carboxylate groups. The dinuclear Zn_2 units are linked to one another by means of tp and bpp linkers to form 2D corrugated sheet (Figs. S9b and S9c) parallel to (−101) (Fig. S9d). The 2D sheets are stacked over each other along [101] in *ABAB* fashion (Fig. S10). The presence of weak C–H···O hydrogen bonding and $\pi\cdots\pi$ interactions (between the aromatic rings of tp and bpp ligands) between two successive 2D layers facilitates the overall supramolecular architecture of **2** ((Table S10 and S11, Figs. 5, S10b and S11). This host framework contains 1D 'virtual' channels along [001], which are filled with disordered guest dmf molecules (Fig. S12).

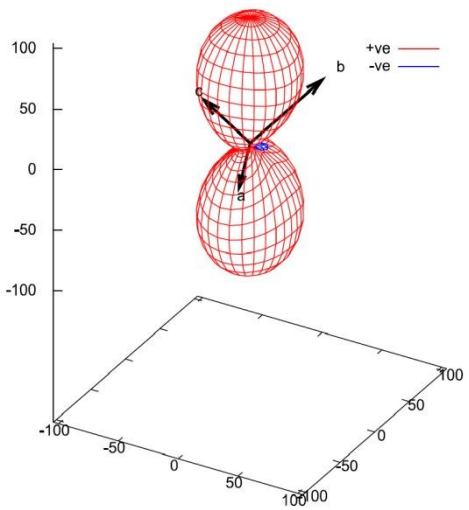

Fig. 6 PASCal[14] expansivity tensor plot for **2**.

VT-SCXRD experiments were carried out to elucidate the temperature-dependent structural changes of **2**. Similar to **1**, SCXRD data were first recorded at 260 K, and then at 20 K intervals down to 100 K. The crystallographic *a* axis contracts significantly upon cooling while the *b* and *c* axes shorten gradually (Fig. S13). Since **2** crystallises in the monoclinic system, the program *PASCal*[14] (Fig. 6) was used to derive a set of orthogonal axes, with corresponding linear thermal expansion coefficients *X1* [–0.5295,0,–0.8483], *X2* [0,1,0] and *X3* [–0.9724,0,0.2332, of –14.7(5), 15.3(5) and 104.1(2) MK^{-1}, respectively. **2** undergoes biaxial positive and uniaxial negative thermal expansion, and the overall volumetric thermal expansion coefficient is 114.9(9) MK^{-1}. The reversibility of the structural response to thermal cycling was also checked (**2_260K-R** in ESI); the initial and final unit cell dimensions at 260 K agree well within experimental error. Variation of the axes *X1*, *X2* and *X3* with temperature is shown in Fig. S14. DSC analysis of **2** shows no thermal event between 100 and 260 K, confirming that **2** does not undergo any phase change (Fig. S6) in this temperature range. TGA shows complete loss of dmf around 215 °C, after which the host is thermally stable up to 350 °C when it starts to decompose (Fig. S7).

To investigate the mechanism responsible for anomalous thermal expansion behaviour of **2** we have analysed the temperature-dependent structural changes and the associated intermolecular interactions. The $\pi\cdots\pi$ distance between the aromatic centroids of the tp and bpp ligands of two adjacent layers decreases continuously with a decrease in temperature (Table S11, Fig. S15). As a result, the $\pi\cdots\pi$ interactions become stronger, leading to contraction of the 2D layer along the *b* axis, and thus contributing to positive thermal expansion along *X2* (Fig. 5b). The contraction is evident as the distance between the Zn^{2+} atoms

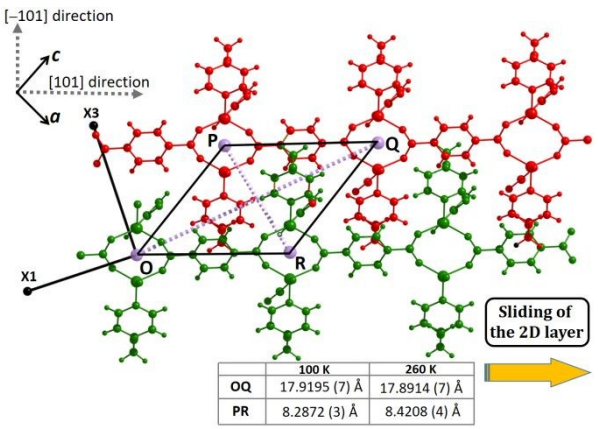

Fig. 7: Perspective view along [010] of the two successive 2D layers of **2**. Upon cooling, the distance between the layers decreases, with concomitant sliding along [101]. These two simultaneous movements result in positive and negative thermal expansion along *X3* and *X1*, respectively.

connected by bpp ligand along the *b* axis (L1 in Fig. 5b) decreases from 10.850(1) Å to 10.776(1) Å upon cooling (Table S12). The angle between two centroids and a Zn atom ($\angle i4$–$i5$–Zn1; θ_2, Fig. S15, Table S11) decreases upon cooling, which indicates that two adjacent 2D layers are encroaching upon each other. Hence, the distance between them along [–101] decreases (Fig. 7). This movement of the 2D layers has an impact on the thermal expansion along *X1* and *X3*. We also note that the C–H···O interactions (Fig. S11) between the non-coordinated carboxylate oxygen atom (O2) and aromatic hydrogen atoms of bpp (C9 — H9···O2) and tp linkers (C7 — H7···O2) become stronger with decreasing temperature

(Table S10). As a consequence of the combined effects of stronger $\pi\cdots\pi$ and C–H···O interactions, two successive 2D layers approach closer (along [−101]), with concomitant sliding along [101] (Fig. 7). As shown in Fig. 7, the distance between the centroids of two secondary building units (SBUs) in two different layers (*i.e.* O and Q) increases with decreasing temperature, resulting in negative thermal expansion along *X1* (Table S13). On the other hand, the distance between the centroids of SBUs P and R decreases with decreasing temperature, which contributes to positive thermal expansion along *X3*.

In conclusion, the co-existence of linear NTE, PTE and ZTE in a single crystal (as observed for **1**) owing to accordion motion has not previously been observed. In **2** the sliding mechanism between the 2D layers interacting via $\pi\cdots\pi$ and C–H···O contacts leads to uniaxial NTE. Discovering and understanding new mechanism whereby materials show anomalous thermal expansion behaviour potentially facilitates better design and development of new thermo-responsive materials.

Acknowledgements

PL gratefully acknowledges financial support from the Department of Science and Technology (DST), New Delhi in the form of a DST-INSPIRE Faculty award [DST/INSPIRE/04/2017/000249]. LJB and AH acknowledge the National Research Foundation of South Africa for financial support.

Notes and references

[a]*School of Chemical Sciences, Goa University, Taleigao Plateau, Taleigao 403206, Goa, India, E-mail: plama@unigoa.ac.in*
[b]*Department of Chemistry and Polymer Science, University of Stellenbosch, Matieland, 7602, Stellenbosch, South Africa, E-mail: ljb@sun.ac.za*

†*Electronic supplementary information (ESI) available: Synthetic procedure, TGA, DSC analysis, detailed crystallographic information and additional figures. CCDC 1947059-1947078. For ESI and crystallographic data in CIF or other electronic format see See DOI: 10.1039/b000000x/*

1 N. W. Ashcroft and N. D. Mermin, *Solid State Physics*, Holt, Rinehart & Winston, 1976.

2 (a) S. Henke, A. Schneemann and R. A. Fischer, *Adv. Funct. Mater.*, 2013, **23**, 5990-5996; (b) H. Aggarwal, R. K. Das, E. R. Engel and L. J. Barbour, *Chem. Commun.*, 2017, **53**, 861-864; (c) H.-L. Zhou, R.-B. Lin, C.-T. He, Y.-B. Zhang, N. Feng, Q. Wang, F. Deng, J.-P. Zhang and X.-M. Chen, *Nat. Commun.*, 2013, **4**, 2534; (d) R. K. Das, H. Aggarwal and L. J. Barbour, *Inorg. Chem.*, 2015, **54**, 8171-8173; (e) B. Dwivedi, A. Shrivastava, L. Negi and D. Das, *Cryst. Growth Des.*, 2019, 19, 2519-2524.

3. P. Lama, R. K. Das, V. J. Smith, L. J. Barbour, *Chem. Commun.*, 2014, **50**, 6464-6467.

4 (a) C. Lind, *Materials,* 2012, **5**, 1125-1154; (b) W. Miller, C. W. Smith, D. S. Mackenzie and K. E. Evans, *J. Mater. Sci.*, 2009, **44**, 5441-5451; (c) Z. Liu, Q. Gao, J. Chen, J. Deng, K. Lin and X. Xing, *Chem. Commun.*, 2018, **54**, 5164-5176; (d) V. K. Peterson, G. J. Kearly, Y. Wu, A. J. Ramirez-Cuesta, E. Kemner and C. J. Kepert, *Angew. Chem., Int. Ed.*, 2010, **49**, 585-588; (e) A. L. Goodwin and C. J. Kepert, *Phys. Rev. B: Condens. Matter Mater. Phys.*, 2005, **71**, 140301-140304; (f) C. Schneider,D. Bodesheim, M. G. Ehrenreich, V. Crocellà, J. Mink, R. A. Fischer, K. T. Butler and G. Kieslich, *J. Am. Chem. Soc.*, 2019, **141**, 10504-10509; (g) E. Pachoud, J. Cumby, C. T. Lithgow and J. P. Attfield, *J. Am. Chem. Soc.*, 2018, **140**, 636-641; (h) C. S. Coates and A. L. Goodwin, *Mater. Horiz.*, 2019, **6**, 211-18

5 (a) A. E. Phillips, G. J. Halder, K. W. Chapman, A. L. Goodwin and C. J. Kepert, *J. Am. Chem. Soc.*, 2010, **132**, 10-11; (b) Z. Ren, R. Zhao, X. Chen, M. Li, X. Li, H. Tian, Z. Zhang and G. Han, *Nat. Commun.*, 2018, **9**, 1638; (c) Y. Song, J. Chen, X. Liu, C. Wang, J. Zhang, H. Liu, H. Zhu, L. Hu, K. Lin, S. Zhang and X. Xing, *J. Am. Chem. Soc.*, 2018, **140**, 602-605; (d) S. Margadonna, K. Prassides and A. N. Fitch, *J. Am. Chem. Soc.*, 2004, **126**, 15390-15391; (e) L. Hu, J. Chen, L. Fan, Y. Ren, Y. Rong, Z. Pan, J. Deng, R. Yu and X. Xing, *J. Am. Chem. Soc.*, 2014, **136**, 13566-13569.

6 (a) Z. Liu, C. Liu, Q. Li, J. Chen and X. Xing, *Phys. Chem. Chem. Phys.*, 2017, **19**, 24436-24439; (b) L. H. N. Rimmer, M. T. Dove, B. Winkler, D. J. Wilson, K. Refson and A. L. Goodwin, *Phys. Rev.* B, 2014, **89**, 214115; (c) A. E. Phillips, G. J. Halder, K. W. Chapman, A. L. Goodwin and C. J. Kepert, *J. Am. Chem. Soc.*, 2010, **132**, 10-11; (d) H.-L. Zhou, Y.-B. Zhang, J.-P. Zhang and X.-M. Chen, *Nat. Commun.*, 2015, **6**, 6917; (e) L. Hu, J. Chen, J. Xu, N. Wang, F. Han, Y. Ren, Z. Pan, Y. Rong, R. Huang, J. Deng, L. Li and X. Xing, *J. Am. Chem. Soc.*, 2016, **138**, 14530-14533. (f) B. K. Saha, S. A. Rather and A. Saha, *Eur. J. Inorg. Chem.*, 2017, 3390-3394.

7 (a) H. Liu, W. Sun, Z. Zhang, X. Zhang, Y. Zhou, J. Zhu and X. Zeng, *Inorg. Chem. Front.*, 2019, **6**, 1842-1850; (b) S. E. Tallentire, F. Child, I. Fall, L. Vella-Zarb, I. R. Evans, M. G. Tucker, D. A. Keen ,C. Wilson and J. S. O. Evans, *J. Am. Chem. Soc.*, 2013, **135**, 12849-12856; (c) J. Li, A. Yokochi, T. G. Amos and A. W. Sleight, *Chem. Mater.*, 2002, **14**, 2602-2606.

8. (a) D. Das, T. Jacobs and L. J. Barbour, *Nat. Mater.*, 2010, **9**, 36-39; (b) K. M. Hutchins, R. H. Groeneman, E. W. Reinheimer, D. C. Swenson and L. R. MacGillivray, *Chem. Sci.*, 2015, **6**, 4717-4722; (c) L. Negi, A. Shrivastava and D. Das, *Chem. Commun.*, 2018, **54**, 10675-10678. (d) D. Das and L. J. Barbour, *CrystEngComm*, 2018, **20**, 5123-5126; (e) V. G. Saraswatula and B. K. Saha, *Chem. Commun.*, 2015, **51**, 9829-9832. (f) S. Bhattacharya and B. K. Saha, *Cryst. Growth Des.*, 2012, **12**, 4716-4719.

9 (a) S. Henke, A. Schneemann and R. A. Fischer, *Adv. Funct. Mater.*, 2013, **23**, 5990-5996; (b) H. Aggarwal, R. K. Das, E. R. Engel and L. J. Barbour, *Chem. Commun.*, 2017, **53**, 861-864; (c) B. K. Saha, S. A. Rather, A. Saha, *Eur. J. Inorg. Chem.*, 2017, 3390-3394; (d) S. R. G. Balestra, R. Bueno-Perez, S. Hamad, D. Dubbeldam, A. R. Ruiz-Salvador and S. Calero, *Chem. Mater.*, 2016, **28**, 8296-8304; (e) Z. Liu, Q. Li, H. Zhu, K. Lin, J. Deng, J. Chen and X. Xing, *Chem. Commun.*, 2018, **54**, 5712-57515.

10 (a) R. Banerjee, H. Furukawa, D. Britt, C. Knobler, M. O'Keeffe and O. M. Yaghi, *J. Am. Chem. Soc.*, 2009, **131**, 3875-3877; (b) J. J. Perry IV, J. A. Perman and M. J. Zaworotko, *Chem. Soc. Rev*., 2009, **38**, 1400-1417; (c) M. Eddaoudi, D.F. Sava, J.F. Eubank, K. Adil and V. Guillerm, *Chem. Soc. Rev*., 2015, **44**, 228-249; (d) S. Sen, S. Neogi, K. Rissanen and P. K. Bharadwaj, *Chem. Commun.*, 2015, **51**, 3173-3176; (e) A. L. Goodwin, M. Calleja, M. J. Conterio, M. T. Dove, J. S. O. Evans, D. A. Keen, L. Peters and M. G. Tucker, *Science*, 2008, **319**, 794-797; (f) J. E. Auckett, A. A. Barkhordarian, S. H. Ogilvie, S. G. Duyker, H. Chevreau, V. K. Peterson and C. J. Kepert, *Nat. Commun.*, 2018, **9**, 4873.

11 (a) E. Yang, X.-C. Song, Y.-D. Lin and S.-Z. Shen, *Acta Cryst.*, 2007, E63, m2067. (b) D.-Y. Ma, K. Lu, L. Qin, H.-F. Guo, X.-Y. Peng and J.-Q. Liu, *Inorg. Chim. Acta*, 2013, 396, 84-91.

12 (a) R. K. Das, H. Aggarwal and L. J. Barbour, *Inorg. Chem.*, 2015, 54, 8171–8173; (b) P. Lama, L. O. Alimi, R. K. Das and L. J. Barbour, *Chem. Commun.*, 2016, **52**, 3231-3234. (c) A. Shrivastava and D. Das, *Cryst. Growth Des.*, 2019, **19**, 4908-4913.

13 (a) L. Liu, B. Geng, S. M. Sayed, B.-P. Lin, P. Keller, X.-Q. Zhang, Y. Sun and H. Yang, *Chem. Commun.*, 2017, **53**, 1844-1847; (b) D. Bléger, Tobias Liebig, R. Thiermann, M. Maskos, J. P. Rabe, and S. Hecht, *Angew. Chem., Int. Ed.*, 2011, 50, 12559-12563; (c) Y. Yoshida, Y. Mawatari, A. Motoshige, R. Motoshige, T. Hiraoki, M. Wagner, K. Müllen and M. Tabata, *J. Am. Chem. Soc.*, 2013, **135**, 4110-4116. (d)

14 M. J. Cliffe, A. L. Goodwin, *J. Appl. Crystallogr.* 2012, **45**, 1321-1329.

TOC Entry

View Article Online
DOI: 10.1039/C9CC06634A

Accordion and Layer-Sliding Motion to Produce Anomalous Thermal Expansion Behaviour in 2D-Coordination Polymers

Prem Lama,*[a] Arpan Hazra[b] and Leonard J. Barbour*[b]

[a]School of Chemical Sciences, Goa University, Taleigao Plateau, Taleigao 403206, Goa, India.
[b]Department of Chemistry and Polymer Science, University of Stellenbosch, Matieland 7602, Stellenbosch, South Africa

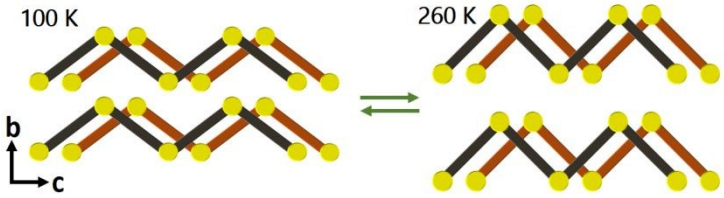

Accordion motion of interwoven 2D layers in 1

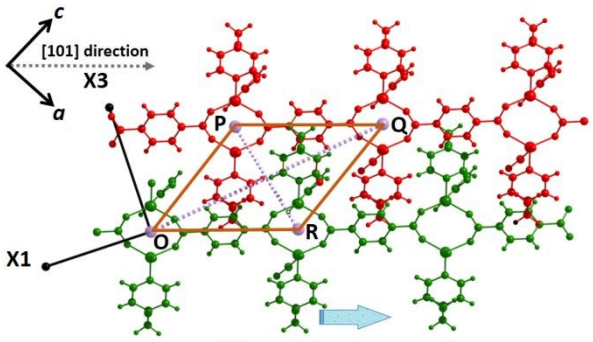

Sliding of the 2D layers in 2

Solvent free (**1**) and solvated (**2**) 2D-coordination polymers have been synthesised by varying the amount of solvent during crystallisation process. The single crystal of **1** shows the co-existence of linear NTE, PTE and ZTE owing to an accordion motion. In **2** the layer-sliding mechanism between the 2D layers due to $\pi\cdots\pi$ and C–H···O interactions leads to uniaxial NTE.